Experimental Section.

Materials. All reactions with air-sensitive materials were conducted under an inert atmosphere using either standard Schlenk techniques or a nitrogen atmosphere glove box. All reagents and solvents were purchased from commercial sources and used as received, unless otherwise stated. *N*,*N*-dimethylformamide (DMF) was refluxed over CaH_2 for 3 days and subsequently distilled prior to use. 18-crown-6 was dried over molecular sieves in CH_2Cl_2, and recrystallized from CH_2Cl_2/hexanes prior to use. $[Fe^{II}(TMCS)]PF_6$ was synthesized according to literature procedures.[S1]

Generation of 2. A THF/DMF (4:1 v/v) solution of **1** (0.2 mM) was cooled to -90 °C. ~50 equiv. (10 μL) of KO_2 (200 mM) dissolved in pure DMF with 18-crown-6 (400 mM) was added to **1** resulting in the immediate (10 s) formation of **2** as evidenced by electronic absorption spectroscopy.

Generation of 3. To a solution of **2** (0.2 mM, THF/DMF 4:1 v/v) at -90 °C was added 2,2,2-trilfuoroethanol (TFE) resulting in the immediate (5 s) disappearance of **2** and the formation of **3** as evidenced by electronic absorption spectroscopy.

Low-temperature UV-vis studies. Electronic absorption spectra were recorded on a Hewlett-Packard (Agilent) 8453 diode array spectrophotometer (190-1100 nm range) in quartz cuvettes cooled using a liquid nitrogen cooled cryostat from Unisoku Scientific Instruments (Osaka, Japan). Molar absorptivity values were calculated by measuring the electronic absorption spectrum of a solution of intermediate **2** generated from a 1 mM solution of $[^{57}Fe(TMCS)]PF_6$ (**1**) and assessing what fraction of the total Fe in the solution is represented by **2** formed by obtaining the Mössbauer spectrum of the same sample. The latter experiment showed that **2** represented greater than 95% of the ^{57}Fe in this solution.

EPR and Mössbauer studies. Mössbauer spectra were recorded using a Janis Research Super-Varitemp dewar that allowed studies in applied magnetic fields up to 8.0 T in a temperature range of 1.5 to 200 K. Mössbauer spectral simulations were performed using the WMOSS software package (SEE Co., Edina, MN). Isomer shifts are quoted relative to Fe metal at 298 K. Perpendicular-mode X-band (9.64 GHz) EPR spectra were recorded on a Bruker EPR 300 spectrometer equipped with an Oxford ESR 910 liquid helium cryostat and an Oxford temperature controller. The microwave frequency was calibrated with a frequency counter and the magnetic field with a NMR gaussmeter. All signals were quantified relative to a Cu-EDTA spin standard. EPR simulations were carried out with a Windows software package (SpinCount) available from Professor Michael Hendrich of Carnegie Mellon University.

XAS Studies. X-ray Absorption Spectroscopy (XAS) data were collected on beamline X3B at the National Synchrotron Lightsource of Brookhaven National Laboratory (NSLS). The synchrotron ring was operated at 2.8 GeV and 100-300 mA beam current and a Si(111) double crystal monochromator was used. The sample (3 mM) was run in fluorescence mode using a 31 element Canberra Ge detector. The sample was maintained at ~ 19 K during data collection. In order to reduce the likelihood of photodecay, no more than three scans were collected on a single spot of the sample, and the edge energy of each scan was determined to verify that no photoreduction occurred. Spectra of an iron foil were collected concomitantly with the samples and were used as internal reference, the first inflection points of which were set to 7112.00 eV.

The software package SSExafs[S2] was used to fit the pre-edge data and the software package EXAFSPAK/FEFF8.4[S3] was used to process the raw XAS data. No channels were excluded from the analysis. No points were excluded from the raw data and no deglitching was performed. Due to a large noise spike at ~ k = 13.8, the k range was restricted to 2-13.5. Fits were generated using the opt program in EXAFSPAK. For a given shell, the coordination number was fixed while the Debye-Waller factor, the bond distance, and the edge shift parameter E_0 were optimized. The scale factor S_0 was set to 0.9.

Reactivity Studies. To a solution of **2** (0.2 mM, THF/DMF 4:1 v/v, generated using ~15 equiv. KO_2) at -90 °C was added 2-methyl-1,4-naphthoquinone (menadione, 20 equiv.) resulting in a reaction that was complete within approximately 60 s affording 2,3-epoxy-2-methyl-1,4-naphthoquinone (menadione epoxide). The yield of menadione epoxide was determined using ^{1}H NMR spectroscopy. The ratio of the CH_3 resonances of menadione (2.13 ppm, TMS as reference) and menadione epoxide (1.66 ppm, TMS as reference) were compared to determine the yields of menadione epoxide after completion of the reaction.

To a solution of **2** (0.2 mM, THF/DMF 4:1 v/v, generated using ~15 equiv. KO_2) at -90 °C was added 2-phenylpropionaldehyde (PPA, 20 equiv.) resulting in an immediate reaction that was complete within 5 s as evidenced by electronic absorption spectroscopy. Acetophenone was identified as the major product in this reaction using GC-MS.

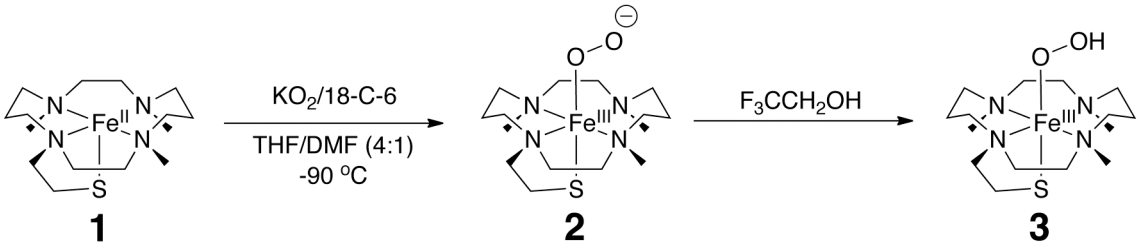

Scheme S1. Reaction between **1** and KO_2 to yield **2**, and the conversion of **2** to **3** with trifluoroethanol.

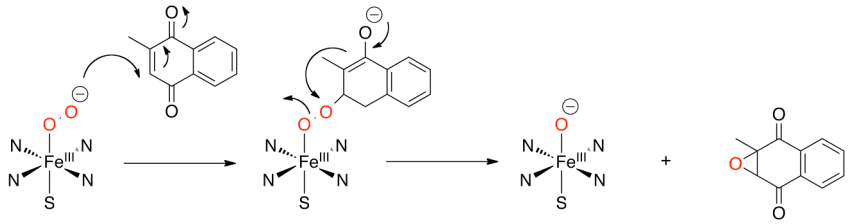

Scheme S2. Mechanism of nucleophilic epoxidation of menadione by **2**.

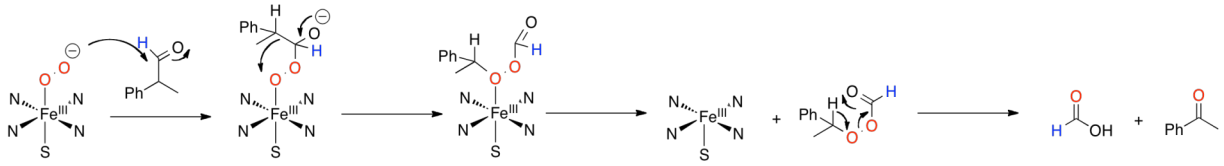

Scheme S3. Mechanism of nucleophilic oxidation of 2-phenylpropionaldehyde by **2**.

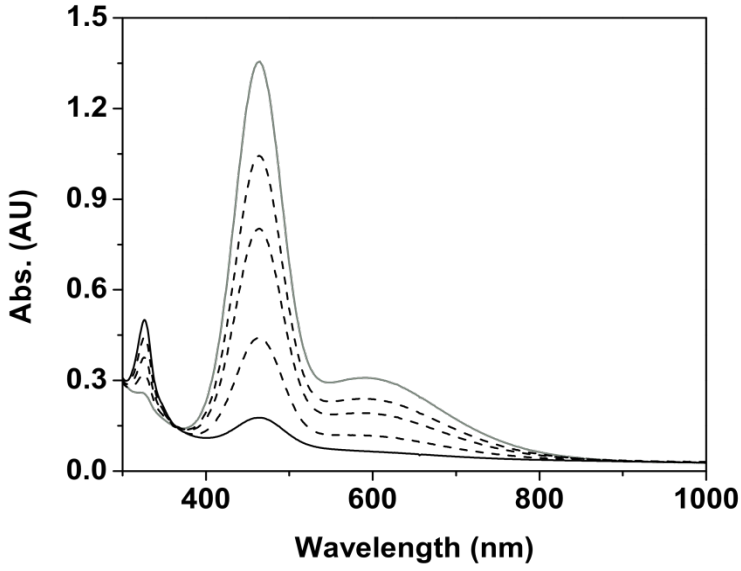

Figure S1. UV-vis spectral changes monitoring the decay of **2** (0.2 mM, gray solid trace) at -90 °C in THF/DMF (4:1) to yield **1** (black solid trace) over the course of 3 h.

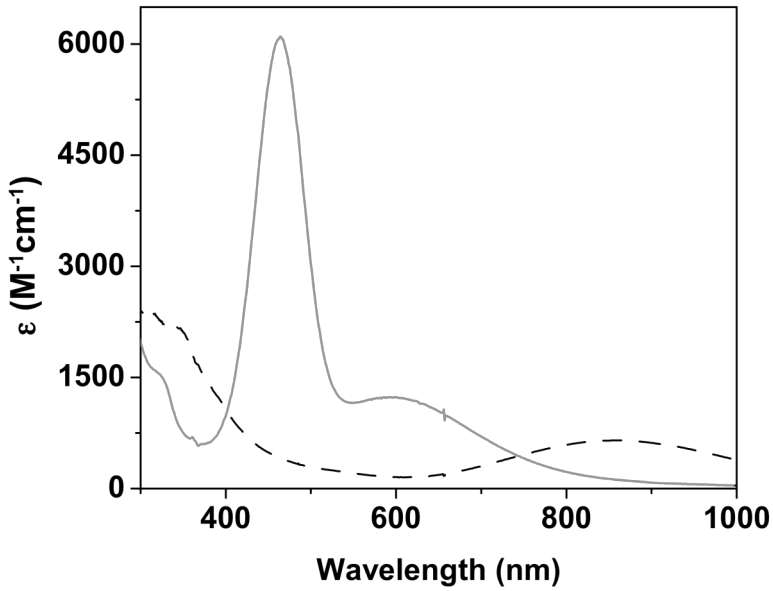

Figure S2. Electronic absorption spectra of $[Fe^{III}(L)(OO)]$ complexes formed from the reaction between $[Fe^{II}(L)]^{+}$ and KO_2 carried out at -90 °C in THF/DMF (4:1). L = TMCS, gray trace; L = TMC/OTf, dashed trace.

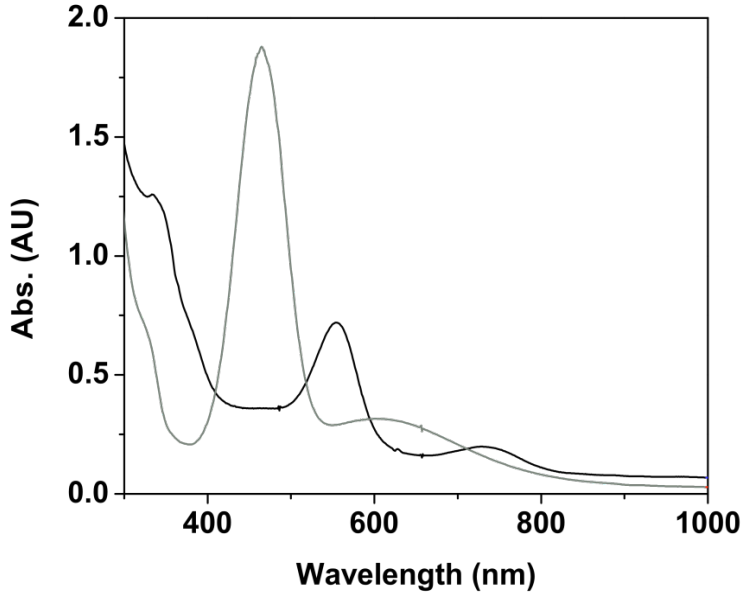

Figure S3. Conversion of **2** (0.3 mM, gray trace) to **3** (black trace) upon addition of 100 equiv. 2,2,2-trifluoroethanol to **2**.

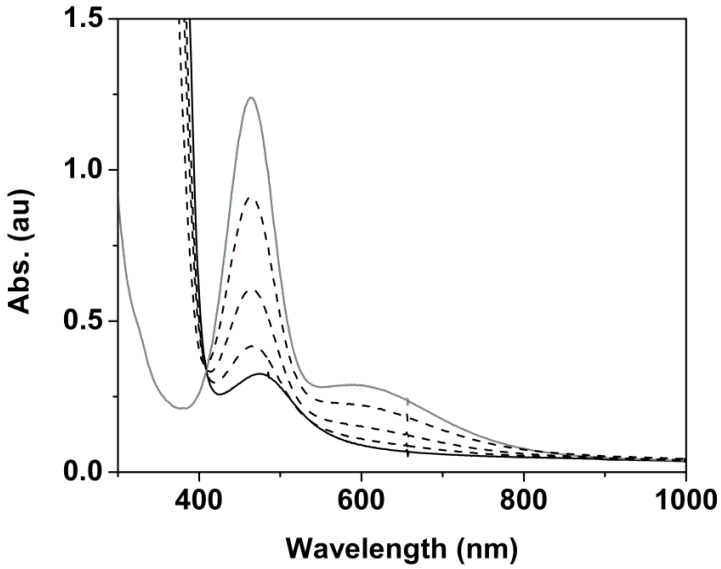

Figure S4. UV-vis spectral changes monitoring the decay of **2** (0.2 mM, gray solid trace) upon exposure to 20 equiv. 2-phenylpropionaldehyde yielding a new RS-Fe^{III} product (black solid trace).

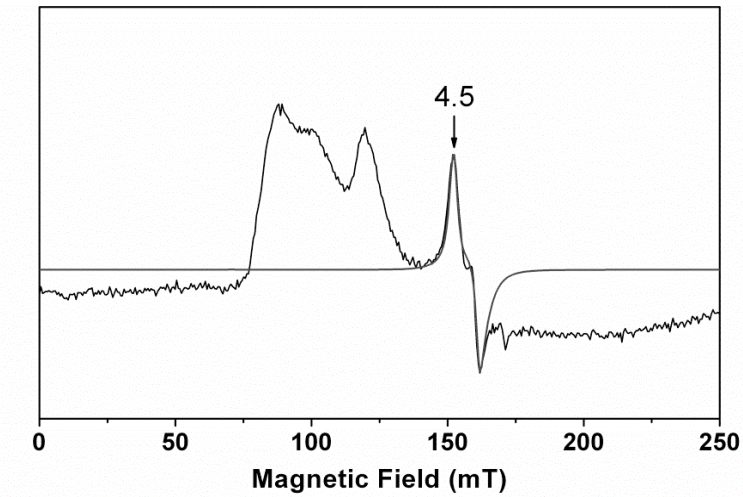

Figure S5. 20 K X-band EPR spectrum of a sample containing **2** in 4:1 THF/DMF frozen solution. The unusual signal at g ~ 4.3 was attributed to a minority Fe species and was quantified to be ~ 0.5% of total Fe in the sample by simulation (gray line) using the $S = 5/2$ spin-Hamiltonian listed in eq. 1 of the main text but with the inclusion of fourth-order ZFS parameters (eq. S1). The parameters used are D = -0.9 cm^{-1}, E/D = 0.295, F = -0.1 cm^{-1}, a = -0.016 cm^{-1}, **g** = (2.03, 2.02, 2), and distributed E/D with σ(E/D) = 0.025. The unique EPR line shape of this species and its parameters identify it as belonging to a previously characterized (η^2-peroxo)iron(III) species.[S4]

$$\hat{H}_{4th} = \frac{F}{180}\left[35\hat{S}_z^4 - 30S(S+1)\hat{S}_z^2 + 25\hat{S}_z^2 - 6S(S+1) - 3S^2(S+1)^2\right] + \frac{a}{6}\left[\hat{S}_x^4 + \hat{S}_y^4 + \hat{S}_z^4 - \frac{1}{5}S(S+1)\left(3S^2+3S-1\right)\right] \quad \text{(S1)}$$

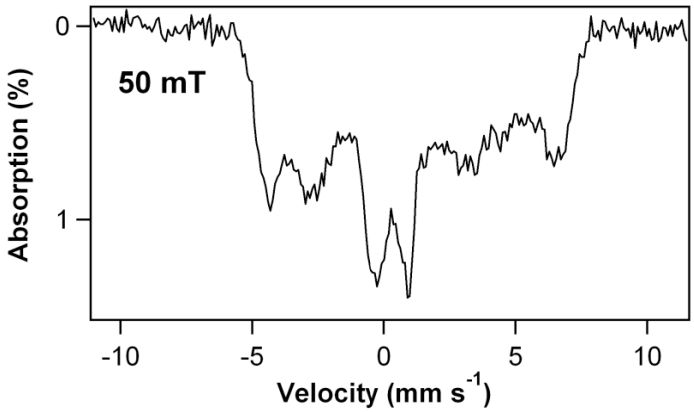

Figure S6. 4.2 K Mössbauer spectrum of **2** recorded in a parallel applied magnetic field of 50 mT.

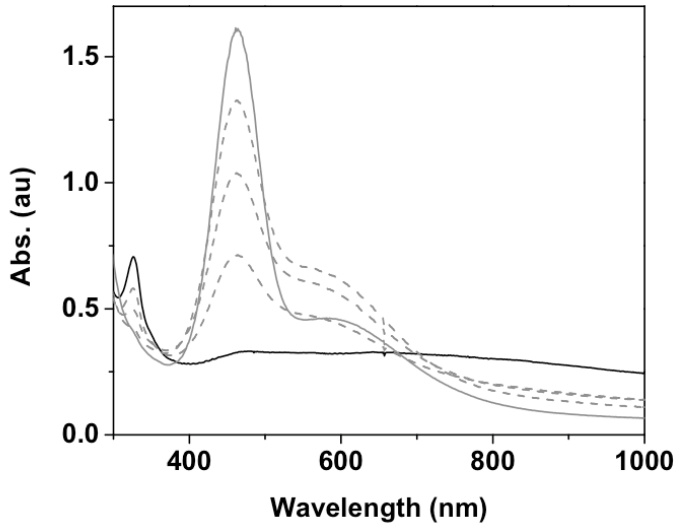

Figure S7. Decay of intermediate **2** (0.25 mM, gray solid trace) upon addition of 100 equiv. MeOH at -90 ºC to yield **1** (black solid trace). A fine precipitate was observed to form that caused a shift in the baseline during the course of this reaction.

XAS Data Analysis of 2

Edge Analysis. The first inflection point of the Fe K-edge occurs at 7123.1 eV, which was taken as the edge energy. The pre-edge region was fit using SSExafs. All parameters were allowed to float freely to obtain the fit show below.

	E_{pk} (eV)	Height	Width	Area
Fit 1	7113.5989	0.029(2)	3.61(28)	11.0(10)

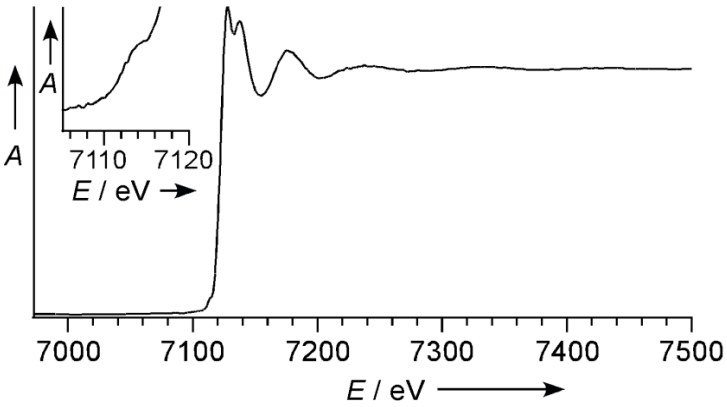

Figure S8. X-ray absorption edge spectrum of **2**. The inset shows the pre-edge region.

EXAFS Analysis. Fits of the unfiltered EXAFS data are reported in Table 2 and are consistent with a six-coordinate species. Four N/O scatterers at 2.17 Å can be attributed to the TMCS ligand. An additional O/N scatterer can be resolved at ~1.9 Å, and the inclusion of this atom dramatically improves the fit, as reflected in the goodness-of-fit parameter F. To determine if the putative peroxo moiety binds in a side-on fashion, 2 O/N scatterers at 1.9 Å were modeled in fits 14-17. In each case, the associated σ^2 value is unreasonably large. The EXAFS data also indicate that the sulfur atom of TMCS remains coordinated to the iron center. As shown in fit 15 of Table 3, the putative Fe–O bond elongates to > 2 Å with an associated large value of σ^2 in the absence of the lower axial sulfur atom, but the fits improve significantly when this scatterer is included. The Fe–S distance of 2.41 Å is slightly longer than the distance of 2.33 Å observed for $[Fe^{IV}(O)(TMCS)]^+$.[S5] The second shell was modeled using carbon scatterers, which can be assigned to the TMCS ligand.

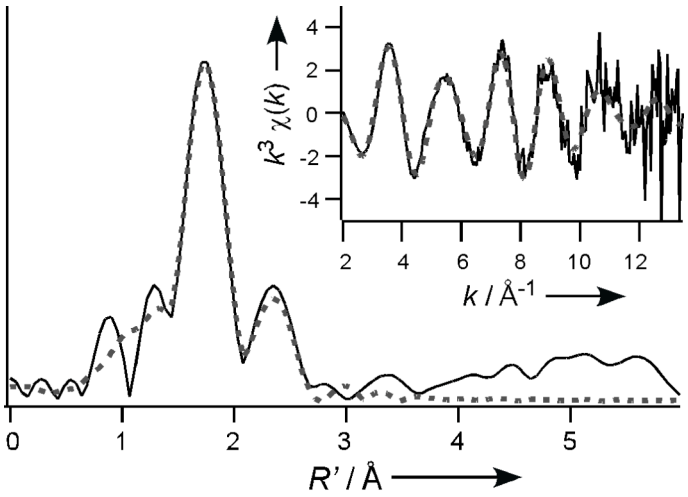

Figure S9. Experimental Fe K-edge unfiltered EXAFS data of **2** (solid line) along with its Fourier transform. Dashed lines indicate fits of the data.

Table S2. EXAFS fitting results for **2** using the unfiltered data, $k = 2 – 13.5$ Å (resolution 0.137 Å).

	Fe-N/O			Fe-S			Fe-O/N			Fe•••C			Fe•••C				
		r			r			r			r			r				
Fit	*N*	(Å)	$\sigma^{2(a)}$	*N*	(Å)	σ^2	*N*	(Å)	σ^2	*N*	(Å)	σ^2	*N*	(Å)	σ^2	E_0	F
1	3	2.23	3.60													1.46	300.3
2	4	2.23	5.14													1.11	275.5
3	5	2.23	6.56													0.76	272.9
4	4	2.22	5.06				1	2.02	50.90							-0.39	
5	5	2.21	6.06				1	1.90	14.67							-2.15	272.1
6	4	2.17	5.23	1	2.41	5.42	1	1.89	6.81							-7.29	266.7
7	5	2.18	7.50	1	2.39	8.52	1	1.88	6.41							-6.05	267.2
8				1	2.27	2.63										-28.84	406.6
				1	2.39	2.25	1	2.14	-1.20							-7.84	295.3
9	4	2.17	5.16	1	2.40	5.24	1	1.89	6.66							-7.60	266.5
10	4	2.17	5.22	1	2.40	5.09	1	1.89	6.43	4	2.97	7.84				-7.48	224.9
11	4	2.17	4.70	1	2.41	5.15	2	1.90	15.75	4	2.97	7.82				-8.17	228.4
12	**4**	**2.17**	**5.31**	**1**	**2.41**	**5.50**	**1**	**1.89**	**7.18**	**4**	**2.93**	**5.62**	**4**	**3.08**	**7.41**	**-6.65**	**212.5**
13	4	2.17	5.31	1	2.41	5.53	1	1.89	7.10	4	2.93	5.37	4	3.08	7.03	-6.69	208.7
													2	3.78	3.67		
14	4	2.22	4.95				2	2.00	48.10							-1.59	277.9
15	4	2.21	4.93				2	2.00	39.10	4	3.02	9.85				-2.82	246.6
16	4	2.21	4.91				2	2.00	37.19	4	2.97	5.67	4	3.14	6.89	-2.95	237.20
17	5	2.21	6.01				2	1.93	29.59	4	2.97	5.59	4	3.13	6.88	-3.28	231.50

Attempted resonance Raman experiments.

Resonance Raman spectra were collected using Kr^+ and Ar^+ lasers (Spectra Physics BeamLok 2060-RM), with excitation wavelengths varying across the visible spectrum (λ_{ex} = 413, 458, 488, 514, 568, 647 nm). Data were collected using an ACTON AM-506M3 monochromator and a LN/CCD-1340 x 400 PB detector. Frozen samples were prepared either on a gold-plated copper cold finger or in NMR tubes. All frozen samples were run at 77 K. Solution samples were transferred to a cooled flat-bottomed NMR tube and run at -90°C.

As vibrational spectroscopy, particularly resonance Raman, is an invaluable tool in distinguishing between peroxo and superoxo ligands, we made repeated attempts to obtain vibrational spectra of **2**. Unfortunately, the 4:1 THF/DMF solvent mixture used to generate **2** forms a glass upon freezing, which interfered with Raman scattering of frozen samples. Our efforts to overcome this problem included freezing samples in NMR tubes at a variety of concentrations in an attempt to facilitate Raman scattering and freezing samples on the surface of a cold finger. We also used a wide range of excitation wavelengths across the visible region (413, 458, 488, 514, 568, 647 nm), and we prepared and analyzed samples using

$K^{18}O_2$. In all cases, Raman scattering was inhibited by the glass. To avoid forming a glass upon freezing, we also investigated the use of other solvent combinations that remained liquid at -90 °C and allowed dissolution of KO_2, but the 4:1 THF/DMF mixture was the only combination that permitted formation of **2**.

The solvent spectra of THF and DMF are also quite complex, with numerous peaks in the spectral region of interest (750 – 1300 cm^{-1}). A noisy baseline, resulting from the glass, prevented us from using a difference spectrum to eliminate spectral contributions from the solvent mixture. The combination of solvents with rich rR spectra and glassing of the sample prevented us from obtaining reliable rR data on frozen samples. Furthermore, the use of $K^{18}O_2$ did not reveal any isotope-sensitive features that could be assigned to **2** (Figure S10).

In an attempt to bypass the problem of glassing samples, we also ran rR experiments using solution samples of **2** maintained at -90 °C. However, we observed a discoloration of the sample during data collection, despite using low power (< 50 mW). The discoloration presumably results from photodecomposition induced by the laser.

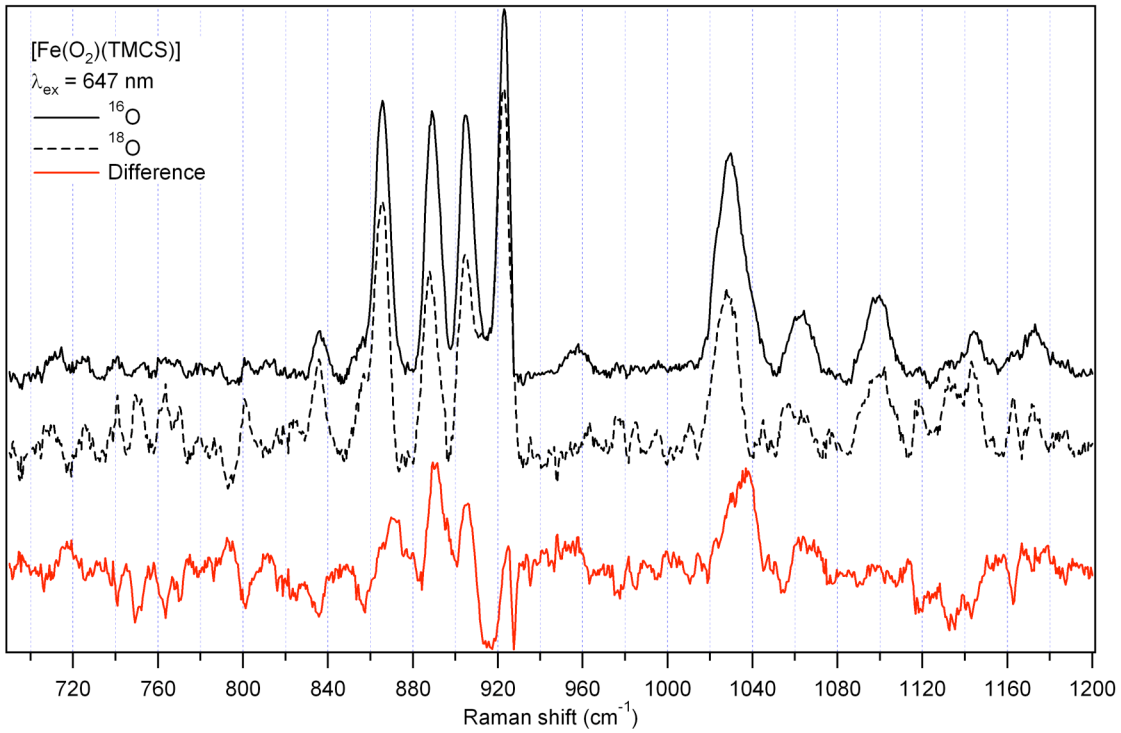

Figure S10. rR spectra of frozen samples of **2** generated with KO_2 (black solid line) and $K^{18}O_2$ (black dashed line) collected at 77 K using 647 nm excitation. The $^{16}O/^{18}O$ difference spectrum is shown in red.

SI references

[S1] A. T. Fiedler, H. L. Halfen, J. A. Halfen, T. C. Brunold, *J. Am. Chem. Soc.,* **2005***, 127*, 1675.

[S2] R. C. Scarrow, M. G. Trimitsis, C. P. Buck, G. N. Grove, R. A. Cowling, M. J. Nelson, *Biochemistry* **1994***, 33*, 15023.

[S3] a) G. N. George, EXAFSPAK; Stanford Synchrotron Radiation Laboratory, Stanford Linear Accelerator Center, Stanford, CA, 2000; b) A. L. Ankudinov, B. Ravel, J. J. Rehr, S. D. Conradson, *Phys. Rev. B* **1998***, 58*, 7565.

[S4] F. Li, K. K. Meier, M. A. Cranswick, M. Chakrabarti, K. M. Van Heuvelen, E. Münck, L. Que, Jr., *J. Am. Chem. Soc.* **2011**, *133*, 7256.

[S5] M. R. Bukowski, K. D. Koehntop, A. Stubna, E. L. Bominaar, J. A. Halfen, E. Münck, W. Nam, and L. Que, Jr., *Science,* **2005***, 310*, 1000.